Imaging Interactions in NGC 4676A/B and NGC 4038/4039

Jay Siri
Group Members: Ellen Min, Meg Wilkinson

Abstract

Galaxy mergers are common in the universe and play a role in the creation of star-forming regions in the galactic life cycle. [7] In this study, we image and analyze two pairs of interacting galaxies in different stages of merging, NGC 4038/4039 (the Antennae Galaxies) and NGC 4676A/B (the Mice Galaxies). Through analysis in various wavelength filters (r', g', i', and Hα), we study both pairs to compare and contrast their levels and regions of activity. We find that NGC 4676A has high levels of activity in its tail, and that the regions near the central bulges of the Antennae Galaxies are likely composed of older stars.

Introduction

Galaxy interaction occurs when galaxies are close (and massive) enough such that their gravitational pull disturbs each other. These interactions perturb the structure of each partner, and cause phenomena such as tidal tails, where the galaxy's matter gets stretched out inversely with the gravitational center of the interaction, and star-forming regions, where matter comes together to trigger new areas of starburst. [7]

To study how galaxy interactions occur and what effects merging has on galaxies, we selected two pairs of mergers and imaged their interactions in different wavelengths. We studied the Antennae Galaxies (NGC 4038/4039), a nearby pair of merging spiral galaxies in a later phase of merging, and the Mice Galaxies (NGC 4676A/B), a similar pair of mergers that are thought to just have begun to interact.

Methods

All data for this study was collected at Palomar Observatory using the Wafer-Scale Imager for Prime (WaSP) instrument, which images in optical wavelengths. [2] We selected, located, and timed our targets using Stellarium. Images were taken in the i', r', g', and Hα filters, and details of our observations can be found in the table below.

Object	**Filter**	**Exposure (sec)**	**Number of Exposures**
NGC 4038/4039	i'	480	1
NGC 4038/4039	r'	120	3
NGC 4038/4039	g'	120	3
NGC 4676A/B	i'	540	3
NGC 4676A/B	r'	420	3
NGC 4676A/B	g'	480	3
NGC 4676A/B	Hα	720	2

To process our data, we took flats in each filter and biases, which were all cropped, median-combined, and average-normalized (and exposure-time-normalized, for the flats) to create "master" flats and biases to be used for data reduction.

To reduce our data, we cropped our raw science frames, normalized by the exposure time, median-combined all the frames, subtracted the master bias, and normalized by the master flat. The final images by filter is shown below.

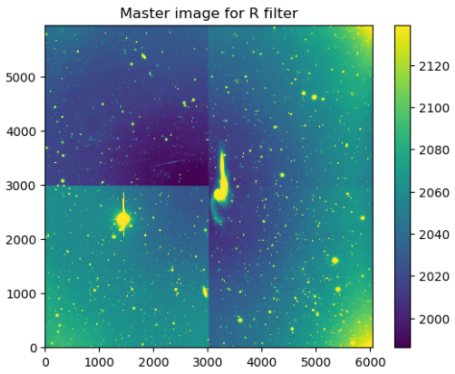

(a) r'.

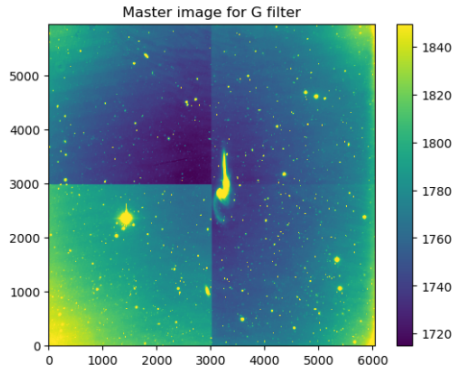

(b) g'.

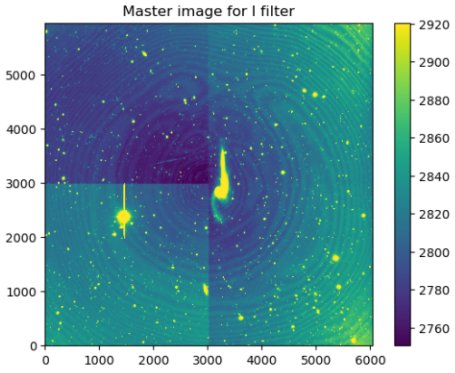

(c) i'.

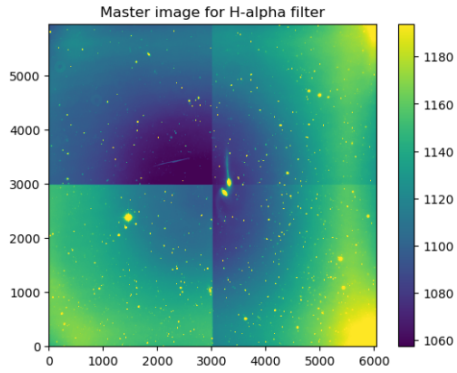

(d) Hα.

Figure 1: Images in each filter for the Mice Galaxies.

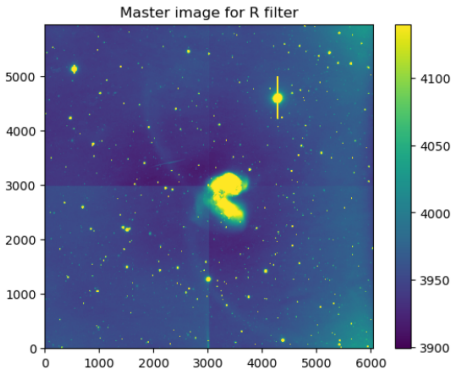

(a) r'.

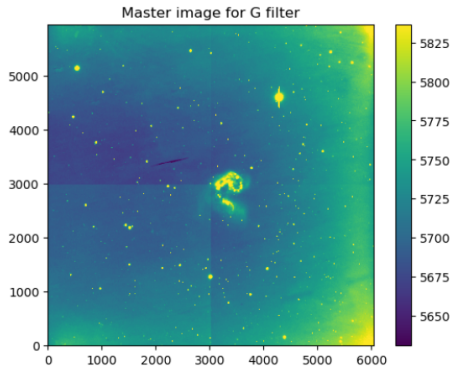

(b) g'.

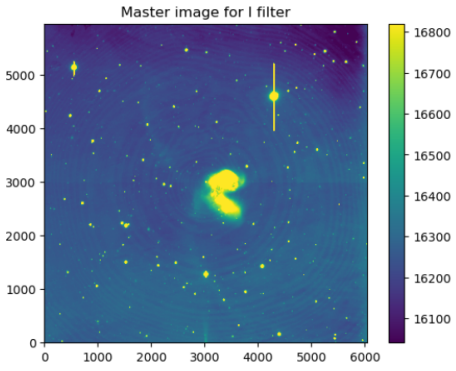

(c) Hα.

Figure 2: Images in each filter for the Antennae Galaxies.

Creating RGB Images

To create Red-Green-Blue (RGB) color images, we rescaled the counts from three different filters and displayed them as an $(M, N, 3)$-shaped array. We experimented with various methods of rescaling, including Lupton *et al.*'s (2004) algorithm and simple linear scaling [6].

Ultimately, we found that square-root rescaling produces the best images. The algorithm is presented below, and was adapted from Min-Su Shin's `myplots` package [3].

```
sqrt_scaling(image_data, scale_min, scale_max):

    """
    This function takes in image data, a min to scale the data to,
    a max to scale the data to, and returns a modified image data
    array with the below transformations applied.
    """

    image_data = image_data.clip(min=scale_min, max=scale_max)
    image_data -= scale_min
    image_data[image_data < 0.0] = 0.0
    image_data = sqrt(image_data)
    image_data /= sqrt(scale_max - scale_min)

    return image_data
```

After rescaling and parameter tuning each of the filter counts, we used `matplotlib`'s `plt.imshow()` function to display I', R', and G'-combined images as a final RGB image.

Tidal Tail Analyses

To compare and contrast the dispersion of matter in different stages of interactions, we studied the clustering of matter in the galaxies' tails as observed in the G' filter. The G' filter permits transmission from 466 ± 140 nm wavelength light, which is towards the higher-energy end of optical wavelengths. Notably, G' transmits the "forbidden" doubly-ionized oxygen lines [O III] at 500.7 nm and 495.9 nm; this ionization requires an already-ionized oxygen atom [O II] to be ionized once more, making it an indicator of energetic activity, including star formation. [4] [5]

We selected the partner with the more prominent tail in both pairs of galaxies (NGC 4676A and NGC 4038) and traced the counts in G' along the tails. For NGC 4676A (the Mice galaxy), we cropped the frame to contain just the galaxy, rectified it, and then got the max counts as a function of distance from the galaxy's center. For NGC 4038 (the Antennae galaxy), this was more difficult to do since the tail was extremely faint in G', there was a lot of background noise and other prominent objects in G', and the tail was curved along a large portion of the sky. Instead, we just fit a second-degree polynomial to the approximate location of the tail and traced the counts along that.

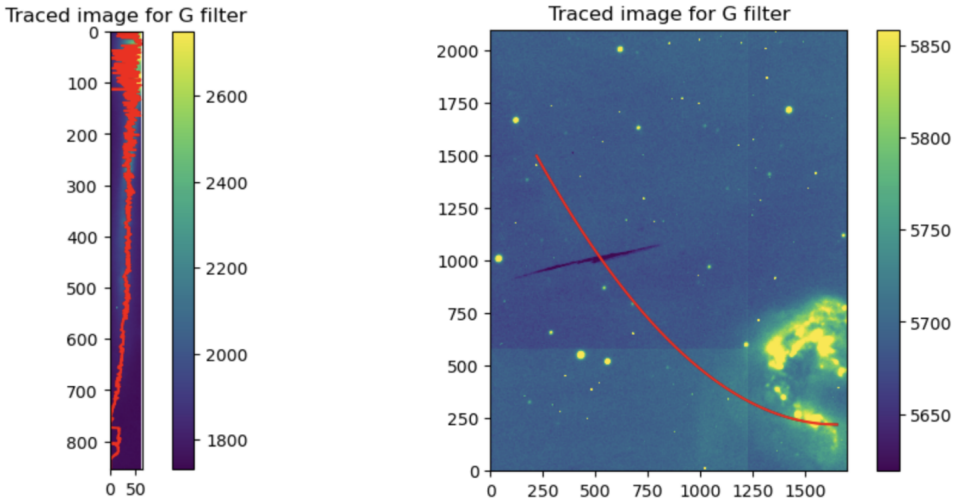

(a) Tail-traced NGC 4676A (Mice) in G'.

(b) Tail-traced NGC 4038 (Antennae) in G'.

Figure 3: Traced count locations (in red) along the tails of the Mice and Antennae galaxies.

H-II Regions in the Mice Galaxies

Our primary method of analyzing star-forming regions in the Mice Galaxies was done with the H-α filter, which transmits light at 657 ± 1 nm, emitted by electron transitions in hydrogen. Since r' encompasses Hα wavelengths, we subtracted normalized Hα counts from r' counts to visualize the regions of star formation.

Photometry of the Antennae Galaxies

We also conducted photometry on bright regions in the Antennae Galaxies to study differences in flux in different filters. To do this, we selected seven notable regions in the Antennae and used a nearby star, HD104456, as a calibration star.

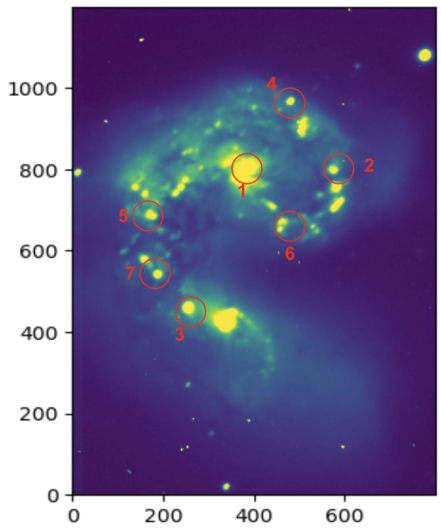

Figure 4: Selected Antennae galaxy regions for photometry.

We found the flux calibration in the r' and i' filters by using HD104456's magnitudes in R and B from the SIMBAD astronomical database to approximate r' and i' magnitudes, and then applied the flux-magnitude relation to convert our counts to magnitudes:

$$m_1 - m_2 = -2.5log_{10}(f_1/f_2)$$

For each of our seven selected regions in the galaxy, we fit a Gaussian using the `lmfit` Python package to select an appropriate aperture, and calculated the total calibrated flux of each region.

Results and Discussion

Our final RGB images, with heavily increased contrast, for both pairs of galaxies is shown below. These images clearly show the areas of interaction between NGC 4038 and 4039, as indicated by the area between the two galaxies with high-energy green regions. In contrast, NGC 4676A/B have no outstanding regions of star formation, though the tail of NGC 4676A is much more pronounced than any of the other galaxies.

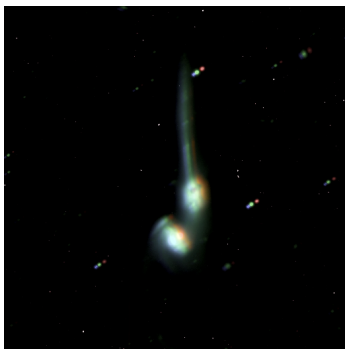

(a) NGC 4676A/B (Mice Galaxies).

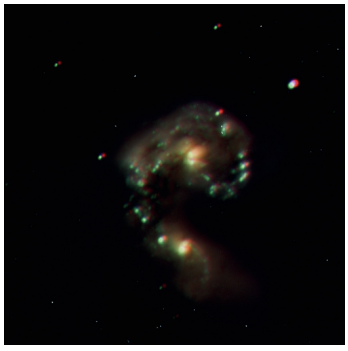

(b) NGC 4038/4039 (Antennae Galaxies).

Figure 5: False color images (using i', r', and g').

Deeper analysis of star formation in the Mice Galaxies is seen using in the Hα wavelength; Figure 6b reveals that star-formation is primarily contained within the galactic central bulges, as expected, but that the tail of NGC 4676A also has significant star formation (located in red).

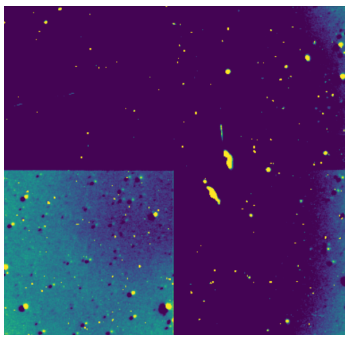

(a) Star-forming regions (Hα minus r').

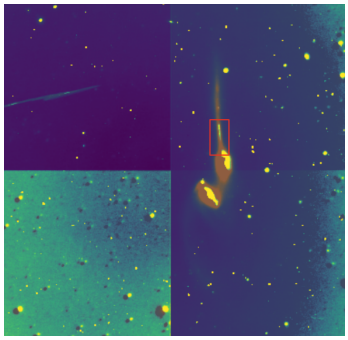

(b) Hα overlayed with star-forming regions.

Figure 6: Star formation in the Mice Galaxies.

This is corroborated by our tidal tail analyses, where counts (in the g' filter) as a function of distance from the galactic center is shown below. By our methodology, Figure 7a (Mice) is much smoother than Figure 7b (Antennae) as expected, but nevertheless Figure 7b shows how low the signal-to-noise ratio between the tail and its surroundings is; the tail of NGC 4038 is not much more active than the background in g'.

Near a pixel count of zero, we expect the counts of both plots to be high since the galactic center is extremely active, but the distinct peaks in Figure 7a in the 200 to 600 pixel region suggests that the tail of NGC 4676A has regions of higher-energy activity. This is thought to be caused by the tail gravitationally collapsing in on itself and triggering activity, which is also suggested by H-II analysis. [1]

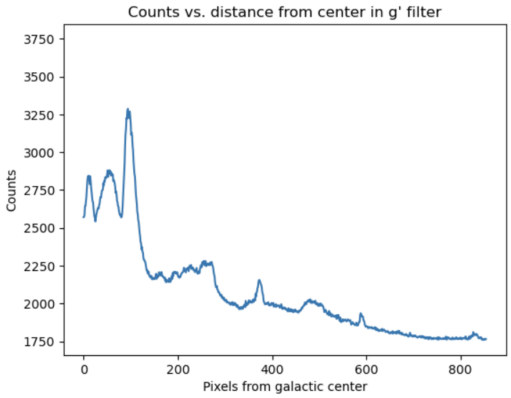

(a) NGC 4676A tail g' counts.

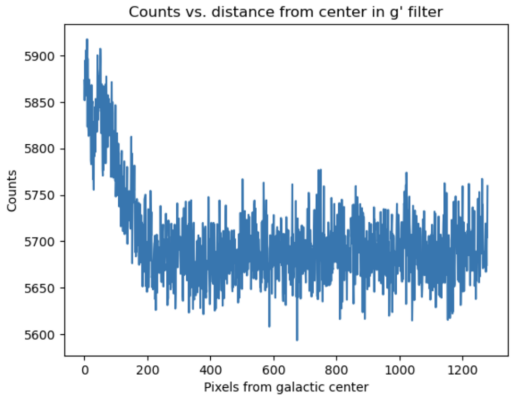

(b) NGC 4038 tail g' counts.

Figure 7: Counts along the tidal tails in g'.

Our photometric analysis of the Antennae Galaxies shows that regions 1 and 3 (as labelled in Figure 4) have a much higher calibrated flux density than the other regions. As seen in the plots below, the color-magnitude diagram created through our photometric analysis in i' and r' filters suggests that these regions are both more red and have higher flux densities than the other regions. This is what we might expect, since these regions correspond to the galactic centers of each partner, which should be compromised of many older, lower-energy stars.

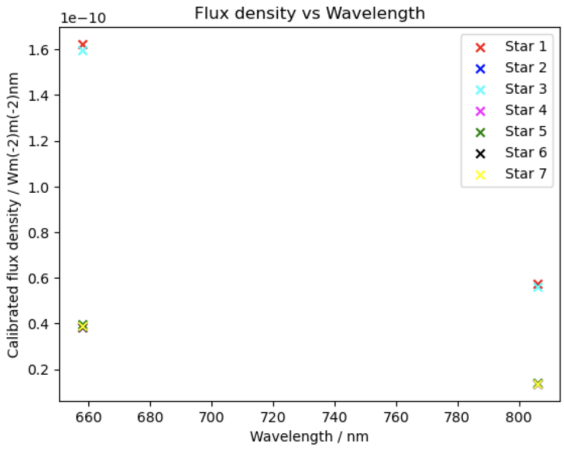

(a) Calibrated flux density (in i' and r').

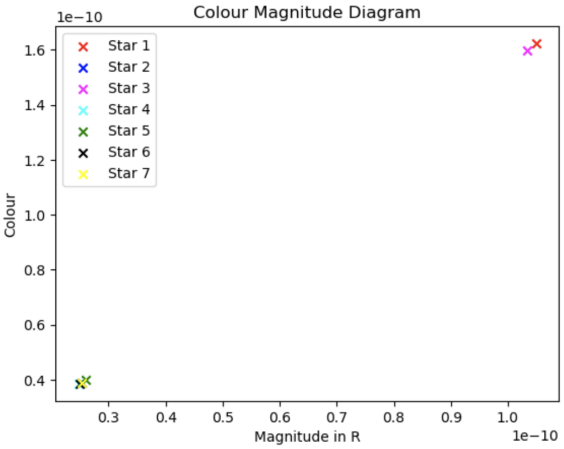

(b) Color-magnitude diagram.

Figure 8: Photometric analyses of regions in the Antennae Galaxies.

Evidently, our analyses produced expected conclusions. Main areas of stellar activity are located near the central bulge of each partner galaxy, although the tail of NGC 4676A is particularly active in comparsion to the very faint NGC 4038(/4039) tail. We conclude by suggesting that future amendments to this study should include an analysis of NGC 4038/4039 in the Hα filter, which we unfortunately did not to image due to logistical constraints. Observing these interactions gives us a deeper understanding of the nature of galaxy mergers and evolution, and ultimately, an understanding of what may be in store for the Milky Way in the future.

References

[1] he Mice (NGC 4676): Colliding Galaxies With Tails of Stars and Gas. `hubblesite.org/contents/media/images/2002/11/1191-Image.html`, April 2002.

[2] Wafer-Scale Imager for Prime (WaSP) Technical Specifications . `https://sites.astro.caltech.edu/palomar/observer/200inchResources/waspspecs.html`, March 2019.

[3] Shin M. `myplots` Python package. `https://github.com/sibirrer/myplots/blob/master/myplots/img_scale.py`, January 2016.

[4] Nakajima; Ellis; Iwata; Inoue; Kusakabe; Ouchi; and Robertson. A Hard Ionizing Spectrum in z = 3 – 4 Ly Emitters with Intense [O III] Emission: Analogs of Galaxies in the Reionization Era? *Astrophysical Journal Letters*, September 2016.

[5] Suzuki; Kodama; Sobral; Khostovan; Hayashi; Shimakawa; Koyama; Tadaki; Tanaka; Minowa; Yamamoto; Smail; and Best. [OIII] emission line as a tracer of star-forming galaxies at high redshifts: comparison between H and [OIII] emitters at z=2.23 in HiZELS. *Monthly Notices of the Royal Astronomical Society*, June 2004.

[6] Lupton; Blanton; Fekete; Hogg; O'Mullane; Szalay; and Wherry. Preparing Red-Green-Blue Images from CCD Data. *The Publications of the Astronomical Society of the Pacific*, February 2004.

[7] Tillman. How the Hubble Space Telescope Changed Our View of the Cosmos. *space.com*, April 2015.